Mass measurements of neutron-rich nuclei near the N=20 and 28 shell closures

B. Jurado, H. Savajols, W. Mittig, N.A. Orr, P. Roussel-Chomaz, D. Baiborodin, W.N. Catford, M. Chartier, C.E. Demonchy, Z. Dlouhý, et al.

Mass Measurements of Neutron-Rich Nuclei Near the N=20 and 28 Shell Closures

B. Jurado[a*], H. Savajols[a], W. Mittig[a], N.A. Orr[b], P. Roussel-Chomaz[a] D. Baiborodin[c], W.N. Catford[d], M. Chartier[e], C.E. Demonchy[a], Z. Dlouhý[c], A. Gillibert[f], L. Giot[a], A. Khouaja[a], A. Lépine-Szily[g], S. Lukyanov[h], J. Mrazek[c], Y.E. Penionzhkevich[h], S. Pita[a], M. Rousseau[a], A.C. Villari[a]

[a]GANIL, BP 5027, 14076 Caen Cedex 05, France

[b]LPC-Caen, ENSICAEN, IN2P3-CNRS et Université de Caen,14050 Caen cedex, France

[c]NPI, ASCR, 250 68 Řež, Czech Republic

[d] Dept. of Physics, University of Surrey, Guilford, GU27XH, UK

[e] Dept. of Physics, University of Liverpool, Liverpool L69 7ZE, UK

[f]CEA/DSM/DAPNIA/SPhN, 91191Gif-sur-Yvette, France

[g]IFUSP-Universidade de São Paulo, C.P. 66318, 05315-970 São Paulo, Brazil

[h]FLNR, JINR, Dubna, P.O. Box 79, 101 000 Moscow, Russia

Mass measurements of very neutron-rich nuclei near the N=20 and 28 shell closures are presented. Seven masses have been determined for the first time and the precision of 36 masses has been significantly improved. These results are used to investigate the evolution of the odd-even staggering of binding energies with neutron number. Special attention is paid to the evolution of the N=28 shell closure as the neutron dripline is approached. Changes in shell structure are observed around N=28 for the P and S isotopes but not for Si. This may be interpreted as a persistence of the shell closure at N=28 or as the result of a very sudden onset in deformation at ^{42}Si.

The mass of a quantum mechanical system, such as the nucleus, is a fundamental quantity as it reflects the sum of all forces acting on it. Of particular interest are direct mass measurements far from the valley of stability (such as those described in this work) which permit tests of the reliability of nuclear mass models to be made and studies of the evolution of shell or subshell closures and correlations to be undertaken. However, the direct measurement of masses far from stability presents significant technical challenges. The principal one being the limited production cross sections. In addition, exotic nuclides are by definition very short lived. The development of a fast measurement technique is therefore imperative, but such technique must also be of sufficiently high resolution to make precision measurements. In the present work we describe how the time-of-flight technique using the SPEG spectrometer [1] at GANIL has been improved in order to determine the masses of very neutron-rich nuclei in the vicinity of N=20 and 28. The results are then used to study the evolution of the odd-even staggering (OES) of nuclear masses with neutron number. When representing nuclear masses as a function of the neutron number one observes that even-neutron-number nuclei are more strongly bound than their odd-neutron-number neighbours. The OES originates from two fundamental physical mechanisms: the breaking of the mean-field spherical symmetry and pairing correlations [2]. Both mechanisms are strongly influenced by the number of neutrons. For instance, it is now well established that de-

*Corresponding author: jurado@cenbg.in2p3.fr, present address: CENBG, F-33175 Gradignan, France

formation effects are responsible for the vanishing of the N=20 shell closure for the very neutron-rich sodium and magnesium isotopes (see, for example, refs. [3–5]). Particle correlations occur mostly in a narrow zone of the phase space around the Fermi surface. In drip-line nuclei the Fermi surface is very close to the single-particle continuum. Consequently, the scattering of virtual pairs into the continuum has to be considered. The increase in neutron-pairing correlations as the neutron binding energy decreases seems to be a quite general result of calculations that include continuum effects (see for example refs. [6–9]). Our results also provide key information to investigate the evolution of the N=28 shell closure when approaching the neutron dripline. Deformation effects and the vanishing of the spin-orbit force could cause an erosion of this shell closure for very neutron-rich nuclei. Finally, our results will be used to check the predictive power of several mass formulas.

For direct mass measurements of exotic nuclei three main issues have to be faced: the production rates, the mass resolution and the systematic errors. A series of earlier mass measurements [10] (and refs. therein) has shown that this can be achieved at GANIL by combining a time-of-flight (TOF) technique with the high-resolution energy-loss spectrometer SPEG. The very broad elemental and isotopic distributions resulting from heavy-ion projectile fragmentation reactions combined with fast in-flight magnetic selection allows the mapping of an entire region of the nuclear mass surface in a single measurement. Compared to other mass measurement methods, the availability at GANIL of very intense neutron-rich beams (such as ^{48}Ca) together with the relatively high transmission rates through the SISSI device [11] and the alpha-spectrometer[2] enables measurements to be made far from stability with reasonable yields. Nuclei with lifetimes as short as the flight time through the system of $\sim 1\mu$s can be measured. The nuclei investigated here were produced by fragmentation of a ^{48}Ca beam of 4 μAe at 60.3·A MeV on a Ta target. The TOF technique requires the simultaneous determination of the masses of well-known nuclei for calibration. Consequently, apart from the neutron-rich nuclei of interest, it is of great importance to measure simultaneously a broad range of reference nuclei. To achieve this, a Ta production target with three different thicknesses and two magnetic rigidities of the beam line and spectrometer were employed. In addition, a thin (25 μm) Be achromatic degrader was placed at the dispersive focal plane of the alpha spectrometer. In this manner, the light ions that caused saturation and pile-up in the detection system in previous measurements were eliminated. As a consequence, the ^{48}Ca beam intensity could be increased by more than one order of magnitude with respect to the previous experiment [10].

The principle of mass determination by means of the TOF technique relies on the relation between the magnetic rigidity, $B\rho$, and the velocity, v, of an ion of rest mass, m_0, and charge, q, traversing an achromatic system: $B\rho = \gamma m_0 v/q$, where γ is the Lorentz factor. A precise measurement of the magnetic rigidity and the velocity allows the ratio m_{0-exp}/q (where m_{0-exp} is the experimental value of the mass of the ion) to be deduced. Once the ion has been identified in A, q and Z, m_{0-exp} can be extracted. The velocity of the ions is obtained from the TOF measurement. Detailed descriptions of the technique may be found in [10] and refs. therein.

The atomic mass excesses are obtained by means of a multidimensional fit where the mass excess is expressed as a Taylor series development of the form (for $q = Z$),
$M^j(A,Z) = Z(m_{0-exp}/Z + \alpha_1^j + \alpha_2^j \frac{A}{Z}) + \alpha_3^j A + \alpha_4^j Z + f_1^j(AZ, A^2, Z^2, \frac{A^2}{Z^2}, A^3, ...) + f_2^j(\Delta E)$

The constant α_1^j and the first order terms serve to transform m_{0-exp} into the atomic mass excess. The function f_1^j, which is a linear combination of higher-order terms in $A, Z, A/Z$ and AZ, and the energy-loss (ΔE) dependent function f_2^j are required to correct for the systematic uncertainties associated with the technique. In contrast to previous experiments where no achromatic degrader was employed, higher order terms were required here to correct for the associated aberrations.

[2] A feature arising from the strong forward focusing of the fragmentation products.

The coefficients of the fit α_i^j are obtained by minimizing the difference between the experimental and the adopted reference mass excesses of the 2003 atomic-mass evaluation [12]. The unknown masses are then determined using the coefficients and functions from the best fit. The uncertainties associated with such a determination arise not only from the statistical uncertainty, but also from the need inherent in the method to interpolate between and extrapole from the reference masses, as well as the systematic uncertainties which are a measure of the limiting precision of the measurement. In the present work a number of *independent* measurements[3] were made resulting in up to 5 independent mass determinations (denoted by the index "j") for many of the nuclei. Each measurement was analysed separately following the procedure outlined above. The uncertainty $\Delta M^j(A,Z)$ for each measurement was determined from the combination in quadrature of the statistical and the systematic errors. The statistical error varied from a few tens of keV for nuclei situated close to the line of stability, to around 1 MeV for nuclei in the vicinity of the neutron dripline where the production rates were very low. The systematic error for each of the measurements was estimated to be 150 keV. The final mass excesses, $M(A,Z)$, quoted in Table 1, are the weighted means of the masses derived from each of the independent measurements. In the present experiment several combinations of higher order terms allowed acceptable fits (as defined by the chi-squared per degree of freedom) to be obtained. The variations in the masses derived from these fits provided a measure[4] of the uncertainty arising from the extrapolations noted above. The uncertainty in the adopted mass excesses (Table 1) was thus derived as the combination in quadrature of that of the weighted mean and that determined for the extrapolation. The results of the analysis described above are listed in Table 1, where seven new masses can be seen to have been determined: ^{23}N, ^{31}Ne, ^{35}Mg, ^{36}Mg, ^{42}Si, ^{44}P and ^{47}Cl. In addition, the precision of 36 masses has been considerably improved with respect to the compilation of ref. [12]. No statistically significant discrepancies between our results and the 2003 atomic-mass evaluation [12] are observed to occur.

The one-neutron separation energy S_{1n} is the most straightforward observable reflecting the OES of binding energies. It is defined as:

$S_{1n}(A,Z) = [M(A-1,Z) - M(A,Z) + M_n]c^2$

where M_n is the neutron mass excess. In order to illustrate the odd-even staggering, figure 1 plots $S_{1n}(N)$ as a function of $S_{1n}(N-1)$ for four isotopic chains. Two diagonal lines can be clearly distinguished. The upper line corresponds to nuclei with an even neutron number (N) for the ordinate which are more strongly bound. The lower line corresponds to nuclei with an even neutron number (N-1) on the abscissa. The separation between the two lines reflects the intensity of the odd-even staggering. Indeed, it is easy to see that if $S_{1n}(N)$=const+δ for even N, and $S_{1n}(N)$=const for odd N, the points formed in a diagram x=$S_{1n}(N-1)$ and y=$S_{1n}(N)$ will lie on two lines, y = x -δ and y = x + δ. The separation between these two lines is then equal to $\delta\cdot\sqrt{2}$. The nuclei with the lowest S_{1n} are the most neutron-rich ones. This original diagram is therefore well suited to trace the dependence of the OES on binding energy. The OES staggering is often taken as an indicator of the strength of pairing correlations. As outlined above, most of the theories including continuum effects predict an increase in neutron pairing correlations with increasing N/Z. However, our results indicate that this does not translate to an increase in the OES. Instead, figure 1 shows an overall reduction of the OES when the binding energy decreases for Z=10 and 12. A strong attenuation of the OES close to the neutron dripline has been predicted for fluorine isotopes by [7]. As described in ref. [7], this does not imply a decrease in the pairing correlations as a decrease in the OES may result from the np-continuum coupling, even if pairing increases. Here, as noted above, we see such a reduction not only for Z = 10, 12 (figure 1) but also for the

[3]These corresponded to runs with different settings of the rigidty of beamline and spectrometer, together with a parallel chain of electronics.

[4]Estimated by calculating the dispersion between the results of the acceptable fits $M^i(A,Z)$ and the final adopted mass excesses – $\Delta M_{ext}(A,Z) = \sqrt{\sum_i (M(A,Z) - M^i(A,Z))^2}$.

	This work	Ref. [12]	Mean
^{23}N	36680(860)		36680(860)
^{23}O	14620(100)	14610(120)	14620(80)
^{24}O	18500(110)	19070(240)	18600(100)
^{25}F	11410(90)	11270(100)	11350(70)
^{26}F	18680(80)	18270(170)	18610(70)
^{27}F	24630(190)	24930(380)	24690(170)
^{27}Ne	7020(70)	7070(110)	7030(60)
^{28}Ne	11280(110)	11240(150)	11270(90)
^{29}Ne	18400(100)	18060(270)	18360(90)
^{30}Ne	23040(280)	23100(570)	23050(250)
^{31}Ne	30820(1620)		30820(1620)
^{31}Na	12520(110)	12650(210)	12550(100)
^{32}Na	18810(120)	19060(360)	18840(110)
^{33}Na	23420(350)	24890(870)	23630(330)
^{34}Mg	8560(90)	8810(230)	8590(80)
^{35}Mg	15640(180)		15640(180)
^{36}Mg	20380(460)		20380(460)
^{34}Al	-3100(80)	-2930(110)	-3040(70)
^{35}Al	-220(70)	-130(180)	-210(70)
^{36}Al	5950(100)	5780(210)	5920(90)
^{37}Al	9810(120)	9950(330)	9830(110)
^{38}Al	16210(250)	16050(730)	16190(240)
^{39}Al	20170(630)	21400(1470)	20360(580)
^{36}Si	-12370(110)	-12480(120)	-12420(80)
^{37}Si	-6620(90)	-6580(170)	-6610(80)
^{38}Si	-4170(70)	-4070(140)	-4150(60)
^{39}Si	2320(90)	1930(340)	2290(90)
^{40}Si	5430(230)	5470(560)	5440(210)
^{41}Si	12120(370)	13560(1840)	12170(360)
^{42}Si	15160(580)		15160(580)
^{40}P	-8030(120)	-8110(140)	-8060(90)
^{41}P	-4980(80)	-5280(220)	-5020(80)
^{42}P	1010(210)	940(450)	1000(190)
^{43}P	4680(370)	5770(970)	4820(346)
^{44}P	9380(900)		9380(900)
^{40}S	-22940(120)	-22870(140)	-22910(90)
^{43}S	-12070(100)	-11970(200)	-12050(90)
^{44}S	-9100(140)	-9120(390)	-9100(130)
^{45}S	-3990(690)	-3250(1740)	-3890(640)
^{43}Cl	-24120(130)	-24170(160)	-24140(100)
^{45}Cl	-18360(100)	-18360(120)	-18360(80)
^{46}Cl	-13810(160)	-14710(720)	-13850(160)
^{47}Cl	-8920(1000)		-8920(1000)

Table 1
Experimental atomic mass excesses (±uncertainties) in keV. In the last column the weighted mean of columns 2 and 3 is given.

oxygen isotopes (not shown). For all the other elements the OES attenuation is less evident and we observe a stabilisation in the OES when approaching the neutron dripline. To illustrate this the Z=13 and 14 isotopic chains are also shown in figure 1, whereby the OES staggering gap is clearly apparent but for the lowest values of S_{1n} the separation between the two groups of data remains rather constant. This indicates that features other than correlations are important. For instance, the spin-isospin coupling, discussed in ref. [13], and thought to be responsible for the deformation effects around N=20, will introduce an effect dependent on the filling of shells.

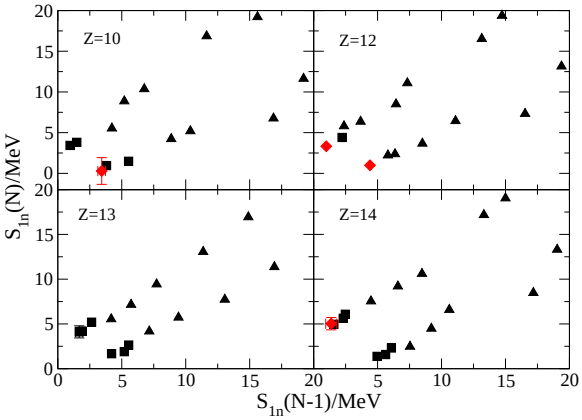

Figure 1. S_{1n}(N) as a function of S_{1n}(N-1) where N is the neutron number. The triangles are from the mass table [12], the diamonds and the squares represent the new and improved (respectively) results measured in the present work.

Several theoretical studies have investigated how to separate the pairing and the mean-field contributions to the OES. The authors of refs. [2,14] proposed to extract the pairing contribution to the OES from experimental data by using the three-point indicator:

$\Delta_3(N)=(-1)^N[M(N-1)+M(N+1)-2M(N)]c^2/2$.

It was demonstrated in ref. [2], that the indicator Δ_3 evaluated for odd-N can be roughly associ-

ated with the pairing effect, while the differences of Δ_3 at adjacent even and odd values of N provide information related to the spacing between single-particle levels, that is, information related to the mean-field contribution. The values of Δ_3 calculated using the experimental masses tabulated in ref. [12] and the results of the present work are displayed in figure 2 as a function of neutron number for four isotopic chains. Let us first consider the case of Ca isotopes (Z=20). As the difference between Δ_3 evaluated at adjacent neutron numbers is sensitive to the single-particle energy differences, it peaks at the magic numbers N=20 and 28. The Δ_3 is almost constant between N=20 and 28 because, for spherical nuclei, the single-particle energy is constant within a shell. At N=Z a strong jump in the Δ_3 is observed for all nuclei, and can be attributed to the Wigner term (see, for example, ref. [15]). The Si isotopes (Z=14) show a very similar behaviour to that of Ca between N=20 and 27, which indicates a regular filling of the $f_{7/2}$ orbital. On the contrary, the behaviour of the P (Z=15) and S (Z=16) chains is different from that of Ca. A local maximum appears at N=26 rather than at N=28. Such an effect at N=26 was already observed in our previous measurement and was attributed to deformation [10]. Owing to the reduction in the uncertainties in the masses for the most neutron-rich P and S isotopes, the effect at N=26 and the vanishing of N=28 as a shell closure have become considerably more apparent than in ref. [10]. Moreover, the present data clearly show that there is no such effect at N=26 for the Si isotopes.

Apart from the effects of deformation, an erosion of the N=28 shell closure could also result from a decrease in the spin-orbit interaction far from stability [16]. The case of ^{42}Si is of particular interest as it could be stabilised against deformation by the Z=14 sub-shell closure. Interestingly, the theoretical predictions for this nucleus are rather contradictory. On the one hand, shell model calculations suggest that ^{42}Si has the characteristics of a doubly-magic nucleus such as ^{48}Ca [17]. The same conclusion was reached in ref. [18], where the deformed configuration was found to be located 1 MeV above the ground state, whereas in other N=28 nuclei (such as ^{40}Mg) the

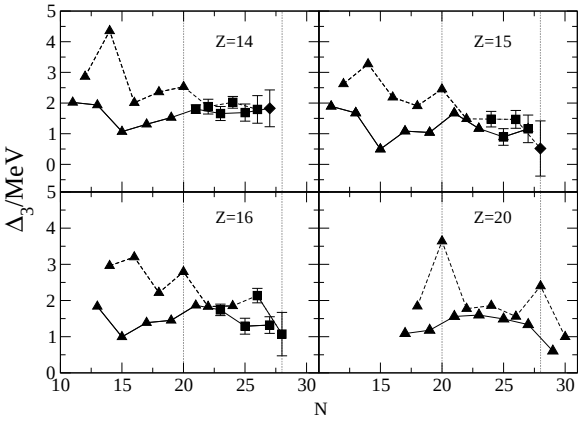

Figure 2. Experimental results for the three-point indicator Δ_3 as function of neutron number. The same symbols are used as in figure 1. The dashed lines link the values of Δ_3 for even-N nuclei and the full lines for odd-N nuclei. The vertical lines indicate the position of N=20 and 28.

deformed intruder state is well below the closed shell. On the other hand, relativistic Hartree-Bogoliubov calculations predict a strong oblate deformed configuration for ^{42}Si [19], in agreement with relativistic mean field calculations with BCS pairing (RMF-BCS) [20] and with the results of the latest version of the Skyrme-Hartree-Fock-Bogoliubov (HFB-9) model [21]. While refs. [19] and [20] predict a rapid transition from prolate to oblate deformation at N=26, for HFB-9 [21] this sudden change in deformation arises at N=28, that is, when going from ^{41}Si to ^{42}Si. From the experimental point of view the situation is rather unclear as well. Grévy et al. have measured the β-decay half-lives of several Si isotopes [22]. The short half-life of ^{42}Si could only be reproduced theoretically assuming a strongly deformed configuration. The present mass measurements of the most neutron-rich Si isotopes are important in order to confirm the conclusions of [22], because the Q_β influences to the fifth power the lifetime. Contrary to the conclusions of ref. [22], high-energy two-proton removal cross sections populating ^{42}Si from a ^{44}S beam were

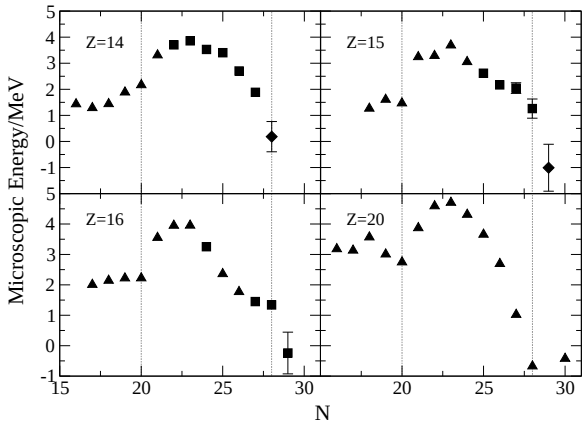

Figure 3. The microscopic correction as function of neutron number. The same symbols are used as in figure 1. The vertical lines indicate the position of N=20 and 28.

interpreted as a signature of the doubly magic character of ^{42}Si [23]. However, in a more recent article it was recognized that the two-proton knockout cross section populating ^{42}Si is not sensitive to the size of the N=28 gap [24]. The mass of ^{42}Si can clearly aid in shedding new light on this question. From the mass measured in the present work one-neutron separation energies of 5.03±0.69 MeV (^{42}Si) and 4.96±0.24 MeV (^{40}Si) were obtained. For the even Si-isotopes, the tabulated S_{1n} decreases by about 1 MeV when going to the next even isotope. One would then expect an S_{1n} of about 4 MeV for ^{42}Si. Our results thus suggest a possible increase in binding as would be expected from a shell closure. Figure 3 represents the microscopic energy as a function of neutron number for the same isotopic chains as in figure 2. The microscopic energy, a convenient quantity to inspect the presence of structure effects in nuclear masses, has been obtained by subtracting the macroscopic component (as given by the Finite Range Liquid Drop Model FRLDM [25]) from the experimental mass excess. The variation of the microscopic energy as a function of neutron number should exhibit deep minima at the shell closures. In figure 3 a strong change in slope at N=20 and near N=28 can be observed for Z=20. However, the Z=15 and Z=16 isotopes do not show such features at N=28 and present instead a discontinuity in the slope at N=26, as observed in our earlier work [10]. This discontinuity is absent for the Z=14 isotopes. The similar behaviour of the microscopic energy for Z=14 and 20 could be considered evidence of a shell closure at N=28, in agreement with the discussion of the OES above. However, in a recent γ-spectroscopy experiment [26] evidence for a low lying 2^+ state in ^{42}Si was found, which is not compatible with such a picture. All these observations could be consistent, however, if deformation effects appear suddenly at N=28.

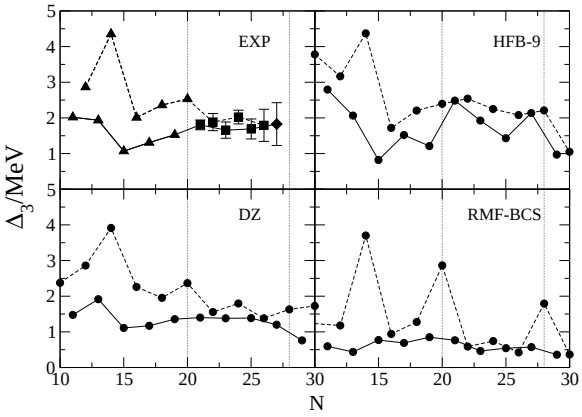

Figure 4. Experimental values of Δ_3 for the Z=14 isotopic chain in comparison with three different mass formulas (see text). The vertical lines indicate the position of N=20 and 28.

Reliable mass formulas that permit extrapolations to the unknown regions of the nuclear chart are important for many domains, such as nuclear astrophysics, and many mass formulas have been developed in recent years [27]. Our results provide new data to test the predictive power of different mass formulas when approaching the neutron dripline. In figure 4 we have compared our experimental values of Δ_3 for the

Si isotopic chain with the HFB-9 mass formula [21], the Duflo-Zuker formula [28], and with the RMF-BCS model [20]. One can see that the best description is given by the Duflo-Zuker formula. This is also true for the other isotopic chains, in agreement with [27]. The HFB-9 model does, for example, not reproduce the shell closure at N=20 and, indeed, for N=21 and 22 it overpredicts the mass. For N >22 the differences between the HFB-9 mass formula and the data decrease. The values of Δ_3 for odd-N derived from the RMF-BCS calculations are systematically lower than the experimental results, probably owing to a weak pairing strength. The predictive power of this model could, therefore, be greatly improved by utilizing a better parametrisation of the pairing. The rms value of the differences between the masses listed in table 1 and the predictions of the FRLDM is 2.721 MeV, for the Duflo-Zuker formula 0.777 MeV, for HFB-9 1.11 MeV, and 1.73 MeV for the RMF-BCS model.

Finally, our results have also been employed to derive a new shell-model parametrisation for the s-d shell Hamiltonians, called USDA and USDB. As a result, a better agreement with experiment for binding energies and excitation energies in the region of ^{24}O has been found, with a reduction of the rms deviation to around 0.13 MeV [29].

In conclusion, we have determined using a direct time-of-flight technique the masses of a broad range of neutron-rich nuclei situated in the vicinity of the N=20 and 28 shell closures. The masses of 7 nuclei have been measured for the first time and the precisions of 36 masses have been considerably improved, in many cases by more than a factor two. These results have been used to explore the evolution of the OES with neutron number, whereby we observe a clear reduction of the OES as the one-neutron separation energy decreases for the Z=8,10 and 12 isotopic chains. This effect needs to be carefully interpreted in order to establish the relative importance of pairing, spin-isospin coupling, and coupling to the continuum which may be needed to explain the observed behaviour. Our results also corroborate the changes in shell structure already observed for the P and S isotopes at the N=28 shell closure. In contrast, such effects are seen to be absent for the Si isotopes. This could indicate either the persistence of the N=28 shell closure for the Si isotopes, or it may reflect a very sudden change in deformation at N=28, as predicted by ref. [21]. To answer this question, ^{42}Si and neighbouring neutron-rich nuclei need to be further investigated. Finally, our results have been used to test and suggest improvements to various mass models as well as derive an improved shell model interaction.

ACKNOWLEDGEMENTS

The authors would like to thank M. Yamagami for fruitful discussions and L. Gaudefroy for carefully reading the manuscript. The untiring efforts of the SPEG crew (J.-F. Libin and P. Gagnant) in preparing the experiment are, as always, gratefully acknowledged as is the effort of the GANIL cyclotron operations group in maintaining a high intensity ^{48}Ca beam and the SISSI device online.

REFERENCES

1. L. Bianchi *et al.*, Nucl.Instrum. Meth. **A276** (1989) 509.
2. W. Satula *et al.*, Phys. Rev. Lett. **81** (1998) 3599.
3. C. Thibault *et al.*, Phys. Rev.**C12** (1975) 644.
4. E.K. Warburton *et al.*, Phys. Rev. **C41** (1990) 1147.
5. Y. Utsuno *et al.*, Phys. Rev. **C64** (2001) 011301(R).
6. J. Okolowicz *et al.*, Phys. Rep. **374** (2003) 271.
7. Y. Luo et al., arXiv: nucl-th/0211068, M. Ploszajczak, priv. comm. and to be published.
8. M. Yamagami, Phys. Rev. **C72** (2005) 064308.
9. M. Matsuo et al., Phys. Rev. **C71** (2005) 064326.
10. F. Sarazin *et al.* Phys. Rev. Lett. **84** (2000) 5062 .
11. W. Mittig, Nucl. Phys. News **1** (1990) 30.
12. G. Audi *et al.*, Nucl. Phys. **A729** (2003) 3.
13. T. Otsuka *et al.* Phys. Rev. Lett. **87** (2001) 082502.
14. J. Dobaczewski *et al.*, Phys. Rev. **C63** (2001) 024308.

15. P. Van Isacker *et al.*, Phys. Rev. Lett. **74** (1995) 4607.
16. G.A. Lalazissis *et al.*, Phys. Lett. **B418** (1998) 7.
17. J. Retamosa *et al.*, Phys. Rev.**C55** (1997) 1266.
18. E. Caurier *et al.* Nucl. Phys. **A742** (2004) 14.
19. G.A. Lalazissis *et al.*, Phys. Rev. **C60** (1999) 014310.
20. L. Geng, PhD Thesis, RCNP Osaka, 2005 unpublished, and Prog. Theor. Phys. **113** (2005) 785.
21. S. Goriely *et al.*, Nucl. Phys. **A750** (2005) 425.
22. S. Grévy *et al.*, Phys. Lett. **B 594** (2004) 252.
23. J. Fridman *et al.*, Nature **435** (2005) 03619.
24. J. Fridman *et al.*, Phys. Rev. **C 74** (2006) 034313.
25. P. Moller *et al.*, At. Data Nucl. Data Tab. **59** (1995) 185.
26. S. Grévy *et al.*, to be published.
27. D. Lunney *et al.*, Rev. Mod. Phys. **75** (2003) 1021 and refs. therein.
28. J. Duflo *et al.*, Phys. Rev. **C52** (1995) R23.
29. B. A. Brown *et al.*, Phys. Rev. **C74** (2006) 034315.